Ultrahigh resolution dissolved organic matter characterization reveals distinct permafrost characteristics on the Peel Plateau, Canada

M. R. N. Moore [ORCID] · **S. E. Tank · M. R. Kurek ·
M. Taskovic · A. M. McKenna · J. L. J. Smith ·
S. V. Kokelj · R. G. M. Spencer**

Abstract The Arctic is warming at a rate twice that of other global ecosystems and changing climate conditions in the Arctic are mobilizing long frozen permafrost stores of organic carbon. In ice-rich regions, permafrost thaw on sloping terrain can cause land subsidence, and the development of thaw-driven mass wasting. The Peel Plateau, Northwest Territories, Canada has extensive thaw-driven landslides called retrogressive thaw slumps that are exposing early Holocene age paleo-thaw layers and Pleistocene age glaciogenic material deposited by the Laurentide Ice Sheet. This study aimed to see if unique retrogressive thaw slump derived permafrost inputs could be readily observed in streams across six diverse thermokarst features via optical and ultrahigh-resolution mass spectrometry. Aquatic samples from water draining thermokarst slump features, and downstream of thermokarst inputs exhibited higher dissolved organic carbon concentrations and lower aromaticity as evidenced by optical parameters (e.g. declining $SUVA_{254}$, increasing $S_{275-295}$) and FT-ICR MS metrics (e.g. lower AI_{mod} and nominal oxidation state of carbon) versus upstream of thermokarst impacts. Increases in the relative abundances of assigned heteroatomic molecular formulae (e.g. CHON, CHOS, CHONS) were also greater within and downstream of thermokarst features. The unique molecular formulae present in permafrost thermokarst inputs were determined ($n = 1844$) and subsequently tracked downstream. These permafrost marker formulae were enriched in aliphatics and H/C, as well as heteroatoms and exhibited low aromaticity. A portion of the unique molecular fingerprint persisted downstream,

M. R. N. Moore (✉) · M. R. Kurek · R. G. M. Spencer
National High Magnetic Field Laboratory Geochemistry Group and Department of Earth, Ocean, and Atmospheric Science, Florida State University, Tallahassee, FL 32303, USA
e-mail: megmoore711@gmail.com

S. E. Tank · M. Taskovic · J. L. J. Smith
Biological Sciences, University of Alberta, Edmonton, AB T6G 2R3, Canada

A. M. McKenna
National High Magnetic Field Laboratory Ion Cyclotron Resonance Facility, National High Magnetic Field Laboratory, Tallahassee, FL 32310, USA

S. V. Kokelj
Northwest Territories Geological Survey, 4601 52nd Ave., Yellowknife, NT X1A 1K3, Canada

highlighting the potential to not only assess thermokarst inputs but also to follow these inputs and their fate downstream throughout the aquatic network.

Keywords Permafrost · Thermokarst · Organic carbon · FT-ICR MS · Arctic

Introduction

Climate change is having a profound impact on Arctic biogeochemical cycles, hydrology, and geomorphology (Kokelj et al. 2021; Littlefair and Tank 2018; Zolkos et al. 2018; Zolkos and Tank 2019). Since 1965, Arctic average surface air temperature has risen about 3 °C exemplifying so called "Arctic Amplification" conditions, wherein the Arctic has experienced warming at a rate twice that of the global average since the 1990's (Biskaborn et al. 2019; Richter-Menge et al. 2019; Schuur et al. 2008). Between 2007 and 2016, permafrost soils have warmed on average about 0.3 °C (Biskaborn et al. 2019), and it is estimated that up to 90% of permafrost that lies close to the surface will be thawed by 2100 (Gruber 2012). There is an estimated 1700 Pg of organic carbon (OC) held in permafrost region soils in the northern high-latitudes, and mobilization and degradation of this well-preserved OC has the potential to further increase atmospheric CO_2 concentrations through a positive feedback cycle (Richter-Menge et al. 2019). Thus, understanding the fate of mobilized permafrost OC is of great relevance to the global carbon cycle due to the size of the permafrost OC store and the rapid pace of its warming and mobilization (Schuur et al. 2008; Report of the Intergovernmental Panel on Climate Change 2021).

About 15% of landmass in the Northern Hemisphere is underlain by permafrost, and about 16% of these permafrost regions are also covered by water features (Obu 2021; Vonk et al. 2015a). In ice-rich terrains, permafrost thaw causes ground subsidence following a reduction in soil or sediment volume associated with melting ground ice, referred to as "thermokarst". In hillslope regions, thermokarst can cause the mass movement of materials downslope, exposing deeper soil layers and enabling transport into recipient aquatic networks. As water interacts with previously frozen soils, dissolved organic matter (DOM) can be mobilized to enter aquatic

environments where it may be degraded via photochemical and microbial processing, or adsorbed onto mineral surfaces (Spencer et al. 2015; Vonk et al. 2015b; Ward et al. 2017; Olefeldt & Roulet 2012). The age of the mobilized dissolved organic carbon (DOC; the carbon component of DOM) can be variable based on its origin, and can range from Pleistocene-aged, to Holocene-aged, through to mobilization from the modern active layer (Lacelle et al. 2013; Drake et al. 2018; Rogers et al. 2021). The introduction of this ancient DOC into contemporary aquatic environments has ramifications for carbon cycling as permafrost thaw DOC has been shown to often be highly biolabile and to be rapidly utilized by microbial communities (Mann et al. 2012; Spencer et al. 2015; Vonk et al. 2015b). However, this input of DOC into aquatic environments may have a wide range of impacts and fates. For example, if mineral soils are also released along with DOC, the DOC can adhere to mineral surfaces and settle out with the sediments, effectively facilitating carbon burial and an overall reduction in DOC concentration (Collins et al. 1995).

Previous work in the Peel Plateau region in northwestern Canada has investigated overall DOC fluxes and biolability of thermokarst slump derived organic matter, as well as particulate organic carbon and inorganic chemistry (Littlefair et al. 2017; Littlefair and Tank 2018; Shakil et al. 2020; Zolkos et al. 2018). Thaw slump size, and the subsequent age of material exposed, are positively correlated with connectivity with downstream locations, and thaw slump size has been increasing over time (Kokelj et al. 2021). The overall impact of thaw slump material additions is dependent on the watershed size, with smaller watersheds experiencing greater impacts proportionally (Kokelj et al. 2021). Previous studies in the Peel Plateau showed Pleistocene aged glacial till deposits that were released from the largest slump sizes were associated with lower DOC concentrations at within-slump locations (Littlefair et al. 2017). This phenomenon was hypothesized to be related to the potential of rapid sorption of the fine-grained inorganic sediments from Pleistocene aged material, to the DOC also released from the retrogressive thaw slump formations. The biolability of thaw slump derived material was shown to be greater than that of unimpacted upstream samples, with less distinction among smaller thermokarst features (Littlefair and Tank 2018). Furthermore, DOM composition was

the primary control of biolability in the Peel Plateau, supporting past studies from Northeastern Siberia, with permafrost sourced material shown to be highly biolabile (Drake et al. 2018; Littlefair & Tank 2018; Spencer et al. 2015). Ultimately, this permafrost sourced DOM has been shown to lead to significant CO_2 outgassing in headwater streams at permafrost thaw impacted sites in Siberia (Drake et al. 2018), and so tracing its inputs and fate is of great importance for our understanding of the changing Arctic carbon cycle.

In previous studies centered on Arctic permafrost samples, a suite of analytical techniques have been used to try to source permafrost DOM inputs including optical parameters at these sites on the Peel Plateau (Littlefair and Tank 2018). Such techniques provide an insight into the bulk optically active portion of the DOM pool but do not have the resolving power of ultrahigh resolution mass spectrometry techniques which have shown the ability to distinguish DOM from a wide range of endmembers including anthropogenic (e.g. agricultural and urban) as well as terrestrial and aquatic sources (Kellerman et al. 2018; Kurek et al. 2021; Vaughn et al. 2021). Fourier transform-ion cyclotron resonance mass spectrometry (FT-ICR MS) has shown the ability, due to its high mass accuracy and resolution, to trace the unique fingerprint of permafrost derived DOM in past studies of yedoma inputs (Drake et al. 2018; Rogers et al. 2021; Spencer et al. 2015). In this study we set out to assess if FT-ICR MS could fingerprint thermokarst DOM inputs on the Peel Plateau. First, we aimed to resolve if permafrost derived DOM exhibits exclusive characteristics, as hypothesized, by examining the DOM composition between upstream and thaw slump derived samples to assess differences in bulk level metrics as well as unique molecular formulae present. Second, we hypothesized these unique characteristics could be tracked downstream and could be used in future studies as a tracer of thermokarst inputs on the Peel Plateau. Such an approach seeks to derive the ability to track future thermokarst DOM inputs by tracking the presence of specific molecular formulae within the DOM pool.

Materials and methods

General site description

The Peel Plateau is located in the continuous permafrost zone of northwestern Canada (Fig. 1). The region is underlain by ice-rich terrain that is comprised of unamended Pleistocene-aged glacial till deposited following the recession of the Laurentide Ice Sheet, overlain by previously thawed Holocene aged materials of several meters thickness into which permafrost was reestablished, and a thin, organic active layer at the ground surface (Duk-Rodkin 1992; Kokelj et al. 2017; Lacelle et al. 2013). The Richardson Mountain range lies to the west and produces a height of land defining the eastward drainage networks that have incised the ice-rich glacial deposits. The westernmost-reaches of the Plateau have exposed bedrock and colluvial deposits and transition through shrub-tundra and eventually subarctic taiga forest in the easternmost reaches (O'Neill et al. 2015). Warming in the early Holocene thawed the upper permafrost layer resulting in the development of Holocene-era soils, which were subsequently frozen as climate cooled and permafrost aggraded (Burn 1997). Warming air temperatures and increased seasonal precipitation has increased contemporary active layer thickness and fluvial erosion, accelerating the growth and development of retrogressive thaw slump features (Kokelj et al. 2015). These rapidly enlarging, chronic landslides can thaw permafrost up to tens of meters thick, and transport previously frozen materials downslope, reconfiguring slopes and fluvial networks (Kokelj et al. 2021). This process mobilizes organic matter into local aquatic ecosystems (Environment Canada 2015; Littlefair et al. 2017), with the contribution of active layer, Holocene-origin, and Pleistocene-origin permafrost dependent in part on thaw slump feature size and depth of permafrost thawed (Kokelj et al. 2021).

Thermokarst slump site selection

Six retrogressive thaw slump (RTS) features were chosen to represent various sizes of RTS present on the Peel Plateau. These sites have been the focus of a number of recent studies examining a range of geochemical impacts (Bröder et al. 2021; Kokelj et al. 2021; Littlefair et al. 2017; Littlefair and Tank 2018;
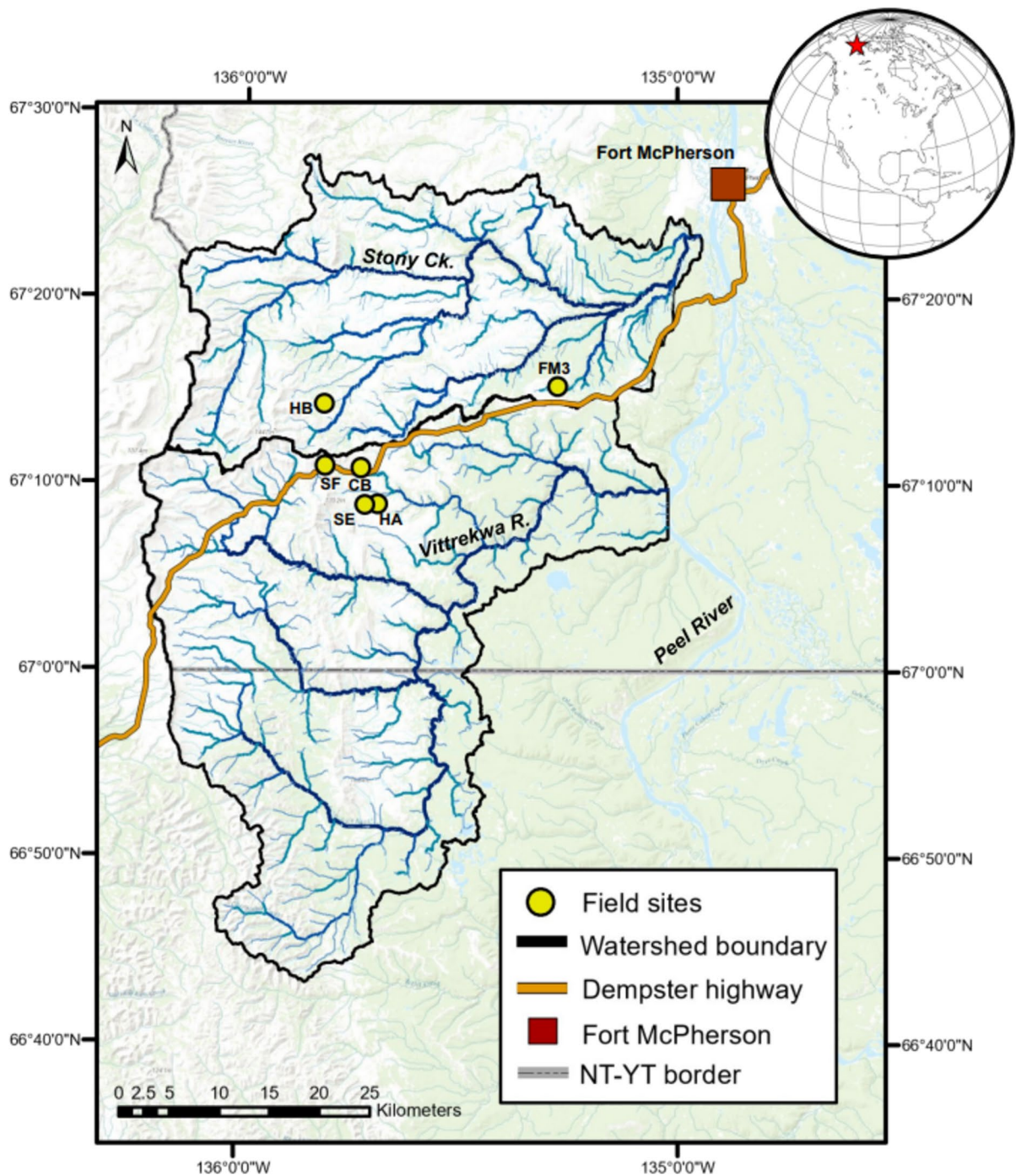
Fig. 1 Location of thermokarst thaw slump sample sites on the Peel Plateau, Northwest Territories, Canada

Shakil et al. 2020). Such RTS features have grown in frequency and areal extent in recent decades in ice-rich permafrost regions and are chronic landslides which grow due to ablation of an ice-rich headwall (van der Sluijs 2023). The chosen slumps are categorized by previously-documented headwall sizes which range from: large size slumps represented by SE (23 m) and FM3 (10.3 m) (Zolkos et al. 2019); medium

size slumps represented by sites HA (7.3 M), HB (7.1 m), and SF (7.6 m) (Zolkos & Tank 2019); and the smaller RTS feature category represented by site CB (5.8 m) (Bröder et al. 2021; Littlefair & Tank 2018; Shakil et al. 2020; Zolkos et al. 2018). Notably, these RTS features also occur across the east–west landscape gradient described above (Fig. 1). The RTS site names utilize the established naming scheme for these sites from past studies (Bröder et al. 2021; Kokelj et al. 2021; Littlefair et al. 2017; Littlefair and Tank 2018; Shakil et al. 2020). At each RTS site, water samples were collected at three locations: upstream of the RTS feature (i.e. control, before the influence of any slump inputs), within-slump runoff water, and downstream from the RTS feature, immediately below the point of all slump inflow.

Field sample collection

Slumps HA, HB, and SE were accessed via helicopter in late June (early season) and early August (late season). Slumps CB, FM3, and SF were accessed by foot, via a road access point from the Dempster Highway in early July (early season) and August (late season) 2021. These slumps were sampled, at three different locations (upstream, within-slump, and downstream), during two seasons (early and late season) except for HA and SF. Due to the inherent challenges of field sampling in Arctic conditions, slump HA was only sampled in the early season, and slump SF was only sampled in the late season. All water samples were collected in 1L acid washed polycarbonate (PC) bottles from just under the stream surface. Sample water was filtered with pre-rinsed 0.45 μm PES filters and the filtered water samples were immediately kept in the dark and subsequently frozen until analysis.

Dissolved organic carbon (DOC) and chromophoric dissolved organic matter analysis

A Shimadzu TOC-V analyzer was used to measure DOC concentrations of samples, and the mean of the best three out of five injections was used with a coefficient of variation < 2% (Littlefair et al. 2017; Murphy et al. 2013). Chromophoric dissolved organic matter (CDOM) absorbance was analyzed using a Biotek EPOCH2 spectrometer for UV–visible absorbance between 250 and 750 nm. Minor interferences were eliminated using a baseline correction procedure

(Green & Blough 1994). The decadic absorbance at 254 nm (m^{-1}) was divided by the DOC concentration (mg C L^{-1}) to calculate the specific UV absorbance at 254 nm ($SUVA_{254}$; L mg C^{-1} m^{-1}). The $SUVA_{254}$ value has been shown to be positively correlated with DOM aromaticity (Weishaar et al. 2003). a_{250}:a_{365} ratios are inversely correlated with DOM molecular size (Peuravuori and Pihlaja 1997) and positively correlated with biolability (Olefeldt and Roulet 2012), and were calculated using established protocols comparing the ratio of the absorbance values between the 250 to 365 nm wavelengths (de Haan and de Boer 1987). The CDOM spectral slope coefficient between wavelengths 275 and 295 nm ($S_{275-295}$; $nm^{-1} \times 10^{-3}$) was calculated using established procedures and has been related to molecular weight and aromaticity with higher values more indicative of smaller, less aromatic DOM (Helms et al. 2008).

Molecular level characterization of dissolved organic matter

DOC concentration values were used to determine the volume of sample required for solid phase extraction procedures as outlined in Dittmar et al. 2008. DOM extraction procedures were aimed to have a target concentration of 40 μg C mL^{-1} and were eluted with 1 mL of methanol. The extracted sample was frozen at − 20 °C before molecular level compositional analysis on a 21 Tesla FT-ICR MS at the National High Magnetic Field Laboratory in Tallahassee, Florida (USA) using negative electrospray ionization (Behnke et al. 2021; Hendrickson et al. 2015; Smith et al. 2018).

The molecular formulae determined by FT-ICR MS analysis were processed using a mass range of 130–1000 *m/z* and noise signals were excluded using > 6 σ root mean square baseline. Molecular formulae were then assigned in the PetroOrg Software (Corilo 2015). Elemental constrains of $C_{4-45}H_{4-92}O_{1-25}N_{0-4}S_{0-2}$ (Kurek et al. 2022b) were used and calculated with no greater than 300 ppb mass accuracy (Behnke et al. 2021). Molecular formulae were divided into functional compound classes based on elemental compositions. The groups used included carbon, hydrogen, oxygen (CHO); nitrogen (CHON); sulfur (CHOS), and sulfur and nitrogen (CHONS). Condensed aromatics ($0.67 < AI_{mod}$), polyphenolics ($0.50 < AI_{mod} < 0.67$), highly unsaturated

and phenolic low O/C (HUP Low O/C, $AI_{mod} < 0.50$, H/C < 1.5, O/C < 0.5), highly unsaturated and phenolic high O/C (HUP High O/C, $AI_{mod} < 0.50$, H/C < 1.5, 0.5 < O/C), and aliphatic (1.5 < H/C) were grouped based on established protocols (Kurek et al. 2022a, b; Šantl-Temkiv et al. 2013).

Statistical analysis

Base R was used with the *ggplot2* package for data analysis and visualization (R Core Team 2019; Wickham 2016), in conjunction with Microsoft Excel, and plotted in MATLAB to create boxplots separated by sampling location to represent minimum, maximum, median, and mean values for DOM optical and compositional variables. A principal component analysis (PCA) was performed on the data using FT-ICR MS and optical derived parameters and visualized using the *factoextra* package in R (Kassambara and Mundt 2017).

Results and discussion

Permafrost slump impacts on DOC and CDOM parameters

Concentrations of DOC in upstream locations ranged from 0.85 to 12.65 mg L^{-1} (mean = 5.19 ± 4.21 mg L^{-1} std dev.; Table 1; Fig. 2a). In all of the box plots, each of the box and whisker shapes represent ten total analyzed samples. Of all upstream locations, the greatest DOC concentrations were found in the early season compared to the matched (i.e. same location) late season sample for all but the SE slump

(Table 1). Within-slump DOC concentrations ranged from 1.45 to 22.85 mg L^{-1} (mean = 10.08 ± 6.89 mg L^{-1}; Table 1; Fig. 2a). The within-slump locations exhibited both the greatest DOC range and mean values when compared to the other sampling locations. The greatest DOC concentrations were found in the late season in all of the within-slump matched pair locations besides slump SE. Downstream DOC concentrations ranged from 1.16 to 13.58 mg L^{-1} (mean = 5.52 ± 2.82 mg L^{-1}; Table 1; Fig. 2a). Of all downstream locations, the highest DOC concentrations were observed in the early season matched pair locations (Table 1).

Previous studies have found a broad range of results regarding DOC impacts from thermokarst features. In East Siberia (Spencer et al. 2015; Vonk et al. 2013) and Alaska (Abbott et al. 2014) slumps significantly increased DOC concentrations in waterways. However, within the Peel Plateau region, DOC concentrations have been previously shown to typically decline downstream of RTS impacted locations, even when within-slump values showed a modest increase in DOC concentrations (Littlefair and Tank 2018). This difference in DOC trends has been attributed to the sorption of RTS released DOC onto inorganic fine-grained, clay rich, glaciogenic sediments during the journey from the RTS complex into the riverine system (Littlefair et al. 2017). Overall, in previous studies in the Peel Plateau region, the DOC range recorded (5.4–26.1 mg L^{-1}) was slightly higher than, but comparable to this study (0.85–22.85 mg L^{-1}) (Littlefair et al. 2017). Variation between the studies is expected as some RTS sites were different than the previous study, which targeted more sites in the easterly, subarctic Taiga reaches of the plateau, and less

Table 1 Average and standard deviations for upstream, within-slump, and downstream permafrost slump locations for DOC and optical parameters for early season (ES), late season (LS), and combined averages (Avg)

Parameter	Upstream ES	Upstream LS	Upstream Avg	Within-Slump ES	Within-Slump LS	Within-Slump Avg	Downstream ES	Downstream LS	Downstream Avg
DOC (mg L^{-1})	6.34 ± 4.16	4.04 ± 4.40	5.19 ± 4.21	10.78 ± 9.04	9.37 ± 4.87	10.08 ± 6.89	6.50 ± 1.72	4.54 ± 3.54	5.52 ± 2.82
a_{250}: a_{365}	5.16 ± 0.94	5.95 ± 0.55	5.55 ± 0.83	6.55 ± 0.66	6.45 ± 0.80	6.50 ± 0.69	6.20 ± 0.98	7.23 ± 0.91	6.71 ± 1.05
$SUVA_{254}$ (L mg C^{-1} m^{-1})	3.45 ± 2.29	1.81 ± 0.49	2.63 ± 1.79	2.03 ± 1.05	1.72 ± 0.63	1.88 ± 0.84	1.31 ± 0.67	1.83 ± 0.53	1.57 ± 0.63
$S_{275-295}$ (nm × 10^{-3})	14.54 ± 1.29	16.50 ± 0.67	15.51 ± 1.42	18.25 ± 1.69	18.09 ± 1.53	18.17 ± 1.52	16.64 ± 1.80	18.43 ± 1.73	17.54 ± 1.92

DOC dissolved organic carbon; a_{250}: a_{365}—ratio of the absorbance values between the 250 to 365 nm wavelengths; $SUVA_{254}$ specific ultraviolet absorbance at 254 nm; $S_{275-295}$ CDOM spectral slope coefficient between wavelengths 275 and 295 nm
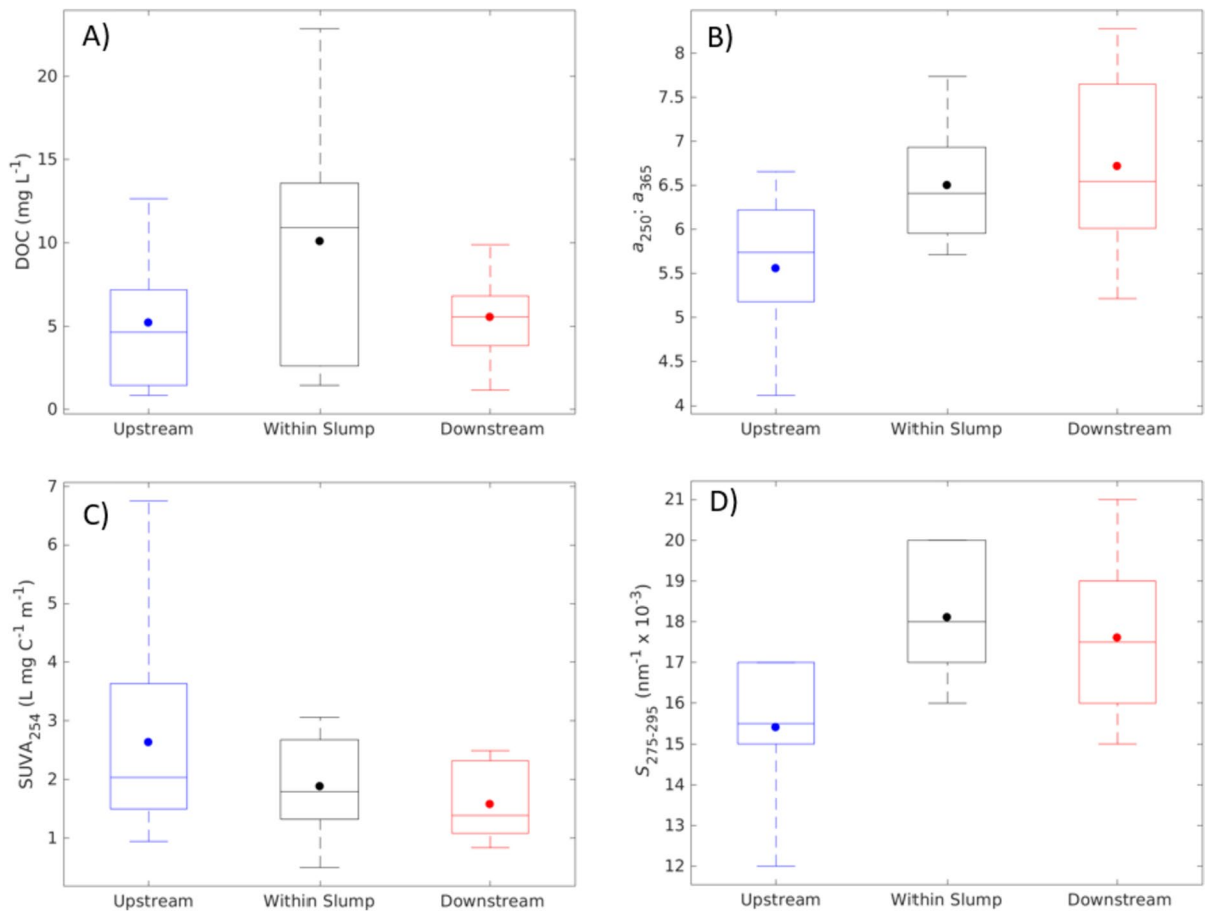
Fig. 2 Box plots representing upstream (blue), within-slump (black), and downstream (red) slump location for (**a**) dissolved organic carbon concentration (DOC), (**b**) a_{250}:a_{365}, (**c**) SUVA$_{254}$, and (**d**) $S_{275\text{-}295}$. Solid circles represent means and horizontal lines represent medians

in the westerly, mountainous reaches. Meteorological conditions on the sampling date also impact DOC concentration, with increased air temperature being positively correlated with DOC concentration (Littlefair et al. 2017).

Ratios of a_{250}:a_{365} for upstream locations ranged from 4.27–6.66 (mean = 5.55 ± 0.83), and from 5.71–7.74 (mean = 6.50 ± 0.69) for the within-slump samples (Table 1; Fig. 2b). Downstream locations ranged from 5.22 to 8.28 (mean = 6.71 ± 1.05; Table 1; Fig. 2b), the largest range and average of all sample locations. At all sample locations, the lowest and highest a_{250}:a_{365} measurements were in the early season (Table 1). CDOM characteristics like a_{250}:a_{365} have been utilized to estimate DOM source and subsequent degradation, as well

as to infer compositional properties of DOM pools (Helms et al. 2008; Peter et al. 2012; Spencer et al. 2007). As a_{250}:a_{365} has been shown to be inversely correlated with molecular weight and directly correlated with biolability of DOM, this highlights the within-slump and downstream locations are expected to be more biolabile than upstream locations (Peuravuori & Pihlaja 1997; Olefeldt & Roulet 2012).

The range for SUVA$_{254}$ in upstream locations was 0.94–6.75 L mg C^{-1} m^{-1} (Table 1; Fig. 2c). The within-slump locations had a smaller range from 0.50 to 3.06 L mg C^{-1} m^{-1}, and the downstream range was even narrower at 0.84–2.48 L mg C^{-1} m^{-1} (Table 1; Fig. 2c). SUVA$_{254}$ values were not substantially impacted by seasonality except

in the upstream sample location, where the greatest $SUVA_{254}$ values were found in the early season (Table 1). $SUVA_{254}$ average values for upstream, within-slump, and downstream got progressively smaller (means $= 2.63 \pm 1.79$, 1.88 ± 0.84, 1.57 ± 0.63 L mg C^{-1} m^{-1} respectively; Table 1; Fig. 2c). Previous studies of $SUVA_{254}$ on the Peel Plateau showed the same relationship, wherein upstream locations had greater $SUVA_{254}$ values indicating that they were more aromatic than within-slump locations (Littlefair and Tank 2018). This aligns with the expected biolability of downstream samples as evidenced by their a_{250}:a_{365} values based on biolability of thawing permafrost trends seen in Eastern Siberian soils with lower MW being associated with greater biolability (Spencer et al. 2015; Vonk et al. 2013). Notably, the upstream $SUVA_{254}$ values from the previous study were generally more than 1 L mg C^{-1} m^{-1} greater than in the current study (Littlefair and Tank 2018). Similar to for DOC concentration, this could be related to the less vegetated nature of the more westerly sample locations in this study (i.e. less vascular plant and litter inputs with elevated aromaticity available for leaching) (O'Neill et al. 2015).

$S_{275-295}$ values ranged from 12.37 to 17.15×10^{-3} nm^{-1} in upstream locations, $16.10–19.96 \times 10^{-3}$ nm^{-1} in within-slump locations, and $15.23–20.60 \times 10^{-3}$ nm^{-1} in downstream locations (Table 1; Fig. 2d). Mean $S_{275-295}$ peaked in the within-slump locations (mean $= 18.17 \pm 1.52 \times 10^{-3}$ nm^{-1}), which were steeper than the upstream locations (mean $= 15.51 \pm 1.42 \times 10^{-3}$ nm^{-1}), and was intermediate for the downstream locations (mean $= 17.54 \pm 1.92 \times 10^{-3}$ nm^{-1}). In both the upstream and the downstream locations, the shallowest values were measured in the early season, and the steepest values were measured in the late season (Table 1). There was limited variability with respect to seasonality in the within-slump locations (Table 1). Steeper $S_{275-295}$ values have been linked with increasing internally produced and/or photodegraded DOM (Helms et al. 2008; Spencer et al. 2012), thus suggesting a less aromatic nature of RTS inputs at the within-slump locations versus upstream locations.

Molecular signatures of permafrost slump dissolved organic matter

Upstream locations had the lowest range of assigned molecular formulae (11,172–14,238) and lower total average number of formulae (mean $= 12,620 \pm 864$; Table 2; Fig. 3a) compared to the within-slump and downstream locations. The within-slump locations had both the greatest range (12,879–18,219) and highest average number of assigned molecular formulae (mean $= 14,650 \pm 15,861$; Table 2; Fig. 3a). Downstream locations exhibited an intermediate range and average (11,314–16,983 and mean $= 13,431 \pm 1701$; Table 2; Fig. 3a). In both the upstream and the downstream locations, the lowest number of assigned formulae were in the early season and the highest number of assigned formulae were in the late season (Table 2). Recent work has highlighted that DOM from more diverse sources typically has a greater number of assigned molecular formulae (Kurek et al. 2023; Textor et al. 2019).

The greatest range in average mass was measured in the downstream locations (467.4236–567.2569 Da, mean $= 520.8625 \pm 28$; Table 2; Fig. 3b), while upstream locations showed the narrowest range (516.5799–573.3658), but the greatest average mass (mean $= 547.4840 \pm 20$) (Table 2; Fig. 3b). The within-slump mass average was the lowest at 510.8770 ± 25 (Table 2; Fig. 3b). These findings are in agreement with previous studies in the Kolyma River Basin, which found permafrost sources had a lower mass average than riverine samples (Rogers et al. 2021). In all sampling locations, the lowest mass averages were found in the early season and the greatest average mass values were found in the late season samples (Table 2).
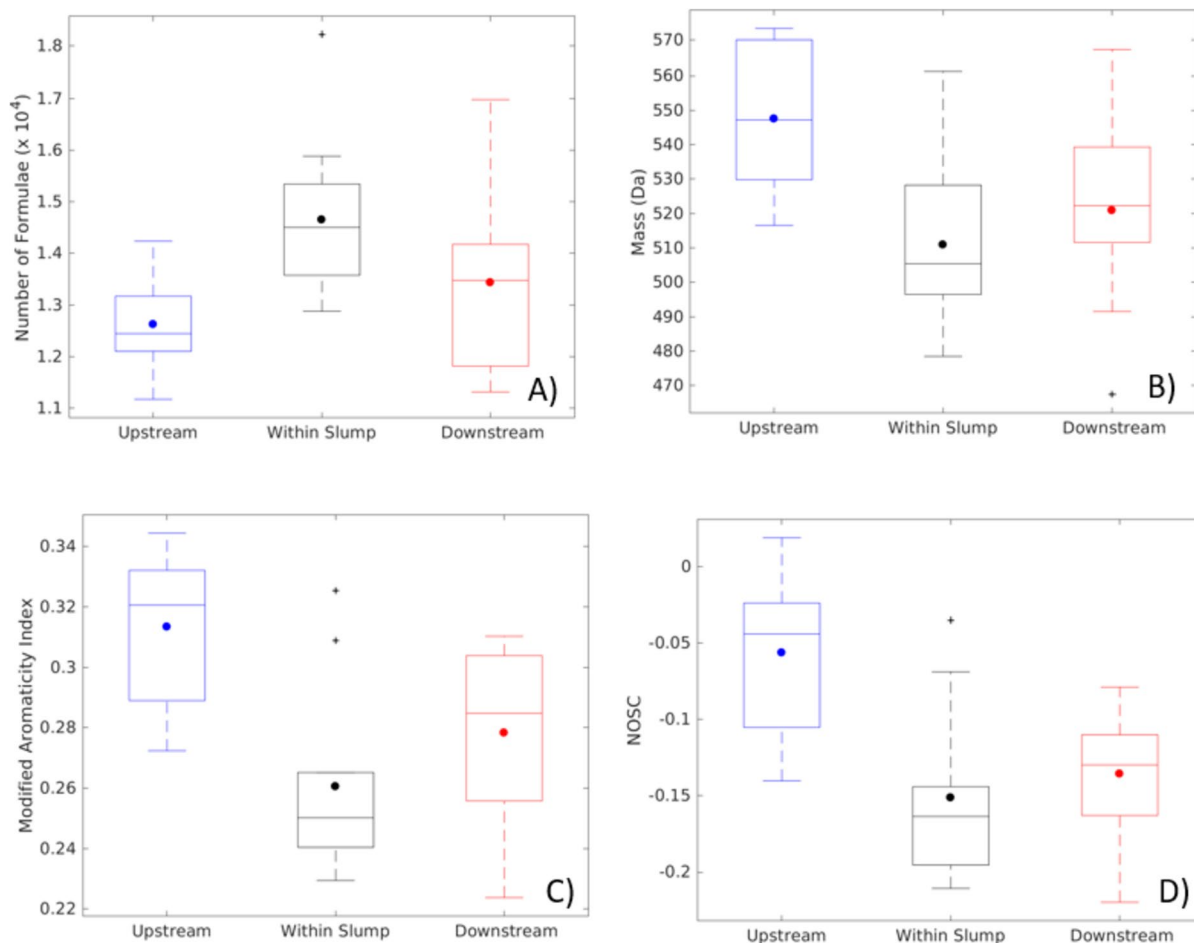
The modified aromaticity index (AI_{mod}), is a parameter derived to highlight aromatic and condensed aromatic formulae in FT-ICR MS spectra (Dittmar et al. 2008), and has previously been shown to be inversely correlated with biolability of molecular formula in permafrost samples (Spencer et al. 2015; Vonk et al. 2013; Textor et al. 2019). The AI_{mod} was greatest for the upstream locations (0.31 ± 0.03) and the lowest in the within-slump locations (0.26 ± 0.03), with the downstream locations falling between the two (0.28 ± 0.03; Table 2; Fig. 3c). These values are similar to results from the Kolyma River Basin which found lower AI_{mod} values associated

Table 2 Average and standard deviations for upstream, within-slump, and downstream permafrost slump locations for FT-ICR MS parameters, for early season (ES), late season (LS), and combined averages (Avg)

Parameter	Upstream ES	Upstream LS	Upstream Avg	Within-Slump ES	Within-Slump LS	Within-Slump Avg	Downstream ES	Downstream LS	Downstream Avg
Number of Formulae	12,489±845	12,752±961	12,620±864	14,869±769	14,430±2224	14,650±1586	12,804±1422	14,060±1871	13,432±1701
Mass (Da)	545.4592±20	549.5087±22	547.4840±20	506.1104±20	515.6435±15	510.8770±25	518.7403±31	522.9848±28	520.8625±28
Modified Aromaticity Index	0.33±0.01	0.30±0.03	0.31±0.03	0.26±0.04	0.26±0.03	0.26±0.03	0.29±0.03	0.27±0.03	0.28±0.03
NOSC	-0.02±0.02	-0.10±0.04	-0.06±0.05	-0.15±0.07	-0.16±0.05	-0.15±0.06	-0.12±0.04	-0.15±0.04	-0.14±0.04
CHO (%RA)	82.6±1.1	81.3±0.90	81.9±1.2	67.6±6.4	73.1±6.9	70.4±6.9	76.6±6.9	74.5±6.1	75.5±6.3
CHON (%RA)	11.3±0.7	10.1±0.9	10.7±1.0	16.9±2.4	14.2±3.1	15.5±3.0	12.9±2.0	13.8±2.7	13.4±2.3
CHOS (%RA)	5.9±1.1	8.2±1.3	7.0±1.7	13.4±5.0	11.2±3.7	12.3±4.3	9.6±4.8	10.4±3.0	10.0±3.8
CHONS (%RA)	0.2±0.2	0.5±0.1	0.4±0.2	2.1±0.9	1.5±1.0	1.8±0.9	0.9±0.8	1.3±0.9	1.1±0.8
H/C	1.07±0.02	1.13±0.03	1.10±0.04	1.18±0.06	1.18±0.04	1.18±0.05	1.14±0.04	1.17±0.04	1.16±0.04
O/C	0.49±0.00	0.47±0.01	0.48±0.01	0.46±0.01	0.46±0.01	0.46±0.01	0.46±0.01	0.46±0.01	0.46±0.01
N/C ($\times 10^3$)	22.4±1.59	21.71±1.74	22.06±1.62	28.21±4.30	25.72±2.73	26.97±3.64	23.54±1.96	25.61±3.90	24.58±3.11
S/C ($\times 10^3$)	7.86±0.82	9.41±0.99	8.64±1.18	15.31±3.91	13.62±3.25	14.46±3.50	11.57±4.91	12.56±3.44	12.06±4.03
Polyphenolics (%RA)	13.4±2.4	8.5±1.8	11.0±3.2	10.2±1.9	9.1±1.3	9.7±1.7	9.8±0.9	8.5±0.8	9.1±1.0
HUP Low O/C (%RA)	36.3±3.8	44.0±1.1	40.1±4.8	40.5±4.8	43.9±3.9	42.2±3.2	42.7±3.0	45.4±3.2	44.1±3.3
HUP High O/C (%RA)	41.2±1.6	38.3±1.5	39.7±2.1	31.2±4.9	31.7±5.6	31.4±5.0	33.8±4.6	31.9±3.7	32.9±4.1
Condensed Aromatics (%RA)	2.4±0.7	1.2±0.5	1.8±0.8	1.7±0.6	1.4±0.3	1.6±0.5	1.6±0.1	1.4±0.3	1.5±0.2
Aliphatics (%RA)	6.8±1.5	8.0±2.2	7.4±1.9	16.4±6.5	13.9±5.2	15.2±5.7	12.1±4.8	12.8±5.4	12.4±4.8

%RA percent relative abundance; *FT-ICR MS* Fourier transform ion cyclotron resonance mass spectrometry; *HUP* highly unsaturated and phenolic, *NOSC* nominal oxidation state of carbon

Fig. 3 Box plots representing upstream (blue), within-slump (black), and downstream (red) slump location for (**a**) number of formulae, (**b**) mean sample mass, (**c**) modified aromatic-ity index (AI_{mod}), and (**d**) nominal oxidation state of carbon (NOSC). Solid circles represent means and horizontal lines represent medians

with permafrost samples when compared to recent vegetation and soil derived riverine samples (Rogers et al. 2021). Seasonality had a modest impact on AI_{mod} values, with early season locations showing a greater AI_{mod} in both upstream and downstream locations, and no effect of seasonality on within-slump average values (Table 2).

Average nominal oxidation state of carbon (NOSC) values were more negative in the within-slump locations (-0.15 ± 0.06), indicating that slump-derived DOM was more reduced than DOM from upstream locations (-0.06 ± 0.05; Table 2; Fig. 3d). A more negative NOSC value is also correlated with less potential energy derived from carbon oxidation per electron (LaRowe and van Cappellen

2011). Downstream locations had NOSC values similar to within-slump locations (-0.14 ± 0.04), but once again fell in between within-slump and upstream location averages (Table 2, Fig. 3d). Late season samples had more negative NOSC values at all sample site locations (Table 2). This suggests that DOM from upstream locations was dominated by oxygenated terrestrial DOM, while DOM from within-slump locations represented a mixture of microbially-derived reduced DOM and degradation products from permafrost thaw inputs (Leewis et al. 2020).

Previous research has shown the relative abundance of CHO assignments comprise the majority of molecular formulae in DOM derived from permafrost soils (Rogers et al. 2021; Spencer et al. 2015).
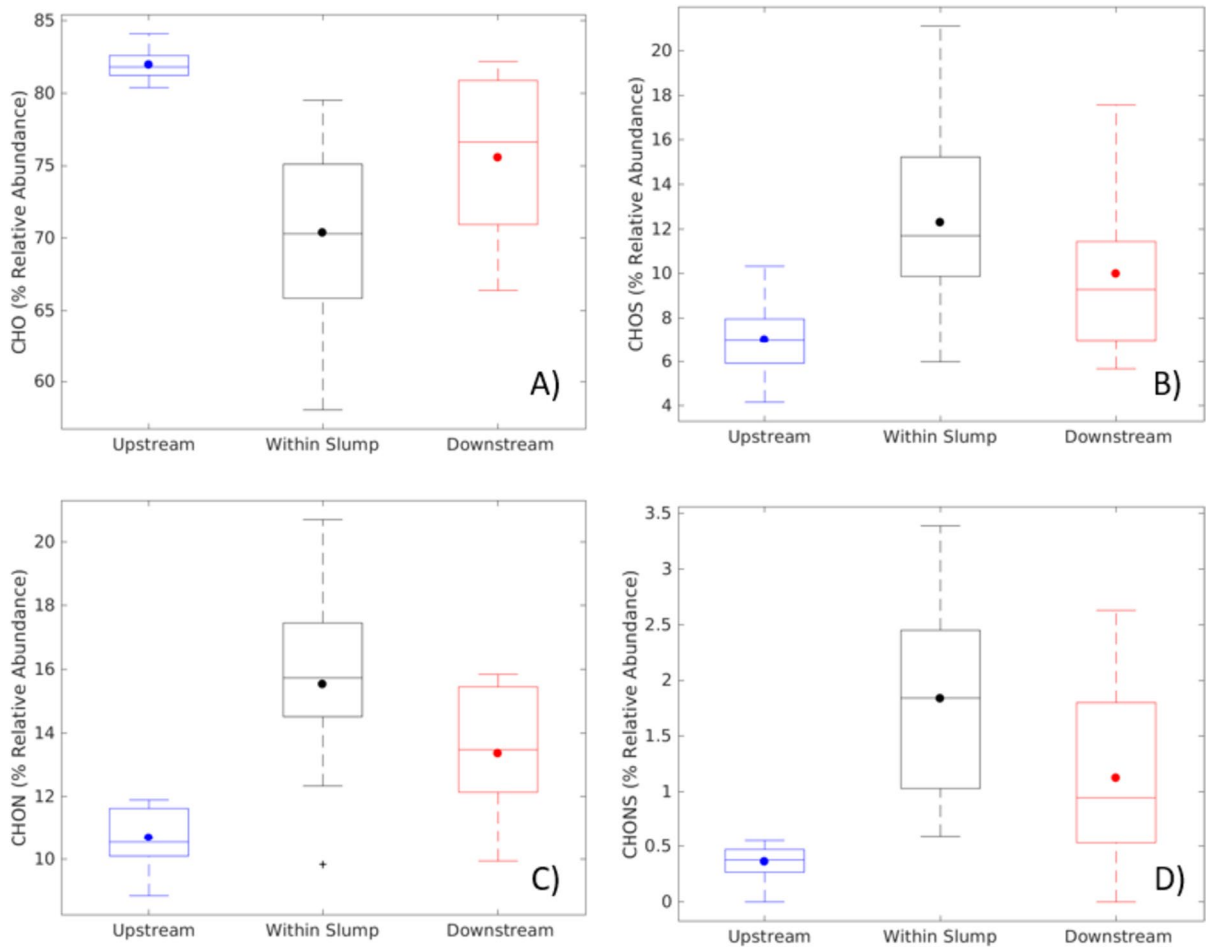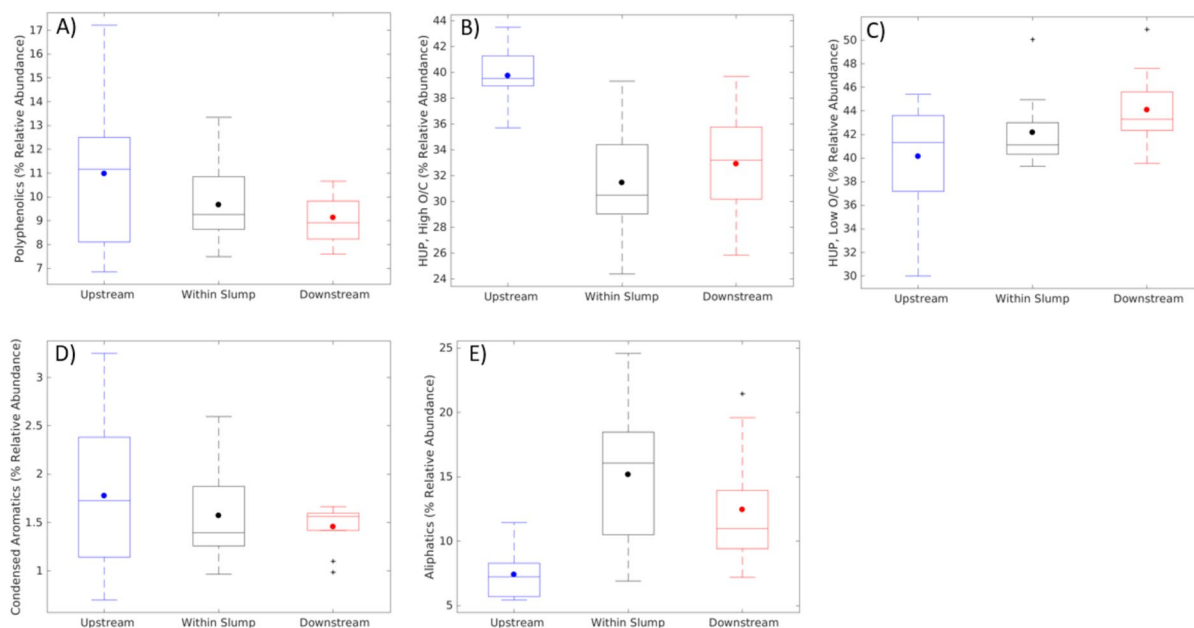
Fig. 4 Box plots representing upstream (blue), within-slump (black), and downstream (red) slump location for relative abundance of (**a**) CHO, (**b**) CHOS, (**c**) CHON, and (**d**) CHONS compositions. Solid circles represent means and horizontal lines represent medians

However, elevated relative abundances of CHOS, CHON, and CHONS formulae have also been found in permafrost samples compared to stream samples dominated by modern terrestrial inputs (Drake et al. 2018; Spencer et al. 2015). On the Peel Plateau, upstream sample locations showed enriched relative abundances of CHO molecular formulae compared to the within-slump locations, and the downstream locations were between the upstream and within-slump ranges (Table 2; Fig. 4a). Within-slump locations showed the greatest relative abundance of CHOS, CHON, and CHONS molecular formulae, while the upstream locations were relatively more depleted with respect to heteroatom containing formulae (Table 2; Fig. 4b–d). The downstream locations once again fell in between the upstream and within-slump

values with respect to heteroatom containing molecular formulae (Table 2; Fig. 4b–d). Limited impact of seasonality was apparent with respect to heteroatom containing formulae throughout the sampling locations (Table 2).

Elemental ratios of H/C, S/C, and N/C were highest in the within-slump locations and lowest in the upstream locations while having the inverse trend for elemental O/C ratios (Table 2). H/C, S/C, and N/C in downstream locations fell in between upstream and within-slump locations, while O/C downstream average was the same as the within-slump average (Table 2). H/C, S/C, N/C and O/C did not show strong or consistent seasonality at any of the sampling locations (Table 2). Elemental N/C ratios are important in the Peel Plateau due to the apparent nitrogen

Fig. 5 Box plots representing upstream (blue), within-slump (black), and downstream (red) slump location for (**a**) polyphenolics, (**b**) Highly unsaturated and phenolic with a high O/C (HUP, High O/C), (**c**) Highly unsaturated and phenolic with a low O/C (HUP, Low O/C), (**d**) condensed aromatics, and (**e**) aliphatics

limited condition of Arctic microbial DOM processing (Littlefair & Tank 2018; Sistla et al. 2012; Wild et al. 2015). Furthermore, greater nitrogen availability is correlated with increased microbial metabolic efficiency which corresponds to more energy used for growth and reduced CO_2 released due to respiration (Mooshammer et al. 2014; Sinsabaugh et al. 2016). Therefore, nitrogen availability can directly impact carbon cycling in Arctic microbial ecosystems. Increased N/C ratios of thermokarst formations in the Peel Plateau is consistent with previous research in the region which found increased N/C ratios to be associated with greater biolability (Littlefair & Tank 2018). Elevated H/C and S/C ratios at the within-slump locations highlight the relative enrichment of hydrogen and sulfur-containing formulae commonly observed in aquatic environments draining from continuous permafrost (Drake et al. 2018; Kurek et al. 2023).

The compound class of polyphenolics has been associated with DOM from aromatic dominated terrestrial sources (Kellerman et al. 2018; Wagner et al. 2015). The greatest range and average for polyphenolic relative abundance was measured in the upstream locations (6.8–17.2%; 11.0 ± 3.2%), with

declining range and averages from within-slump (7.5–13.3%; 9.7 ± 1.7%) to downstream (7.6–10.7%; 9.1 ± 1.0%; Table 2; Fig. 5a). Early season averages for polyphenolic relative abundances were greater than late season averages at all sampling locations (Table 2). The highly unsaturated and phenolic grouping with a high O/C ratio (HUP high O/C) showed the lowest averages in the relative abundance in the within-slump (31.4 ± 5.0%) locations and the greatest average in the upstream locations (39.7 ± 2.1%), and the downstream average fell in between (32.9 ± 4.1%; Table 2; Fig. 5b). The greatest relative abundance of HUP high O/C averages values were in the early season for upstream and downstream samples, while seasonality did not greatly impact within-slump averages (Table 2). The highly unsaturated and phenolic grouping with a low O/C ratio (HUP low O/C) showed the greatest relative abundance average in the downstream locations (44.1 ± 3.3%) with descending averages from within-slump to upstream locations (42.2 ± 3.2; 40.1 ± 4.8; Table 2; Fig. 5c). HUP low O/C averages were the greatest in the late season at all sampling locations (Table 2).

The relative abundance of condensed aromatics, indicators of highly aromatic terrestrial DOM

Table 3 PCA correlation matrix

DOC	− 0.42	− 0.41
$a250: a365$	− 0.79	0.13
$SUVA_{254}$	0.51	− 0.36
$S275-295$	− 0.91	0.12
Number	− 0.58	− 0.28
Mass	0.68	0.31
CHO	0.92	0.35
CHON	− 0.72	− 0.54
CHOS	− 0.90	− 0.15
CHONS	− 0.91	− 0.31
Condensed Aromatics	0.47	− 0.80
Polyphenolics	0.63	− 0.76
HU Low O/C	− 0.39	0.82
HU Hi O/C	0.93	0.01
Aliphatics	− 0.93	− 0.23
AImod	0.94	− 0.12
NOSC	0.93	− 0.22

DOC dissolved organic carbon; a_{250}: a_{365} ratio of the absorbance values between the 250 to 365 nm wavelengths; $SUVA_{254}$ Specific ultraviolet absorbance at 254 nm; $S_{275-295}$ CDOM spectral slope coefficient between wavelengths 275 and 295 nm; *HUP* highly unsaturated and phenolic; *NOSC* Nominal Oxidation State of Carbon

(Kellerman et al. 2018; Wagner et al. 2015), were less defined by sample location, but the upstream locations had the greatest average (1.8 ± 0.8%), the downstream locations had the lowest average (1.5 ± 0.2%), and the within-slump locations fell in between (1.6 ± 0.5%; Table 2; Fig. 5d). The early season had the greatest condensed aromatic relative abundance averages at all sampling locations (Table 2; Schmidt et al. 2009; Sleighter and Hatcher 2008). The greatest average values of polyphenolic, HUP high O/C, and condensed aromatics in the unimpacted upstream locations thus highlights relatively greater terrestrial, more aromatic inputs at these sites. A similar trend has been shown in streams in Siberia between permafrost thaw dominated and modern terrestrial DOM dominated sites (Drake et al. 2018), as well as past research at these upstream locations has shown them to have greater modern terrestrial inputs (Littlefair et al. 2017).

The compound class of aliphatics has been linked to DOM from in situ production and microbial sources and is related to elevated biolability (Kurek et al. 2023; Spencer et al. 2015; Textor et al. 2019). Within-slump sample locations showed the most
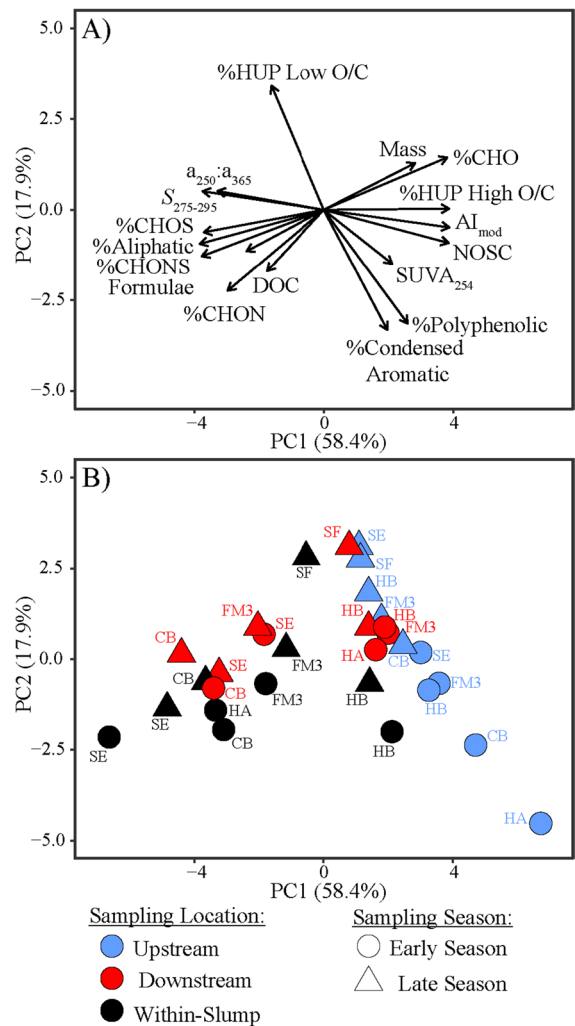
Fig. 6 a Principal component analysis functions showing trends within the data, where the vectors convey the magnitude of their impacts. **b** The specific sample locations within the PCA space are mapped with circles representing early season and triangles representing late season samples. The blue corresponds to upstream samples, black with within-slump samples, and red with downstream sites

enriched average aliphatic content (15.2 ± 5.7), and upstream sample locations showed the most depleted average aliphatic content (7.4 ± 1.9), with the downstream values falling in between upstream and within-slump averages (12.4 ± 4.8; Table 2; Fig. 5e). There were limited impacts with respect to seasonality on aliphatic content for all sample locations (Table 2).

Fig. 7 van Krevelen diagrams of **a** formulae present in all upstream samples (upstream common), **b** formulae present in all within-slump samples (within-slump common), **c** formulae found in all within-slump samples, but not in the upstream samples (within-slump unique: WSU), **d** the within-slump unique formulae that persist downstream (within-slump unique in downstream: WSUD), **e** Venn diagram of unique and common formulae for upstream, within-slump, and downstream locations; the number of formulae in each group is included
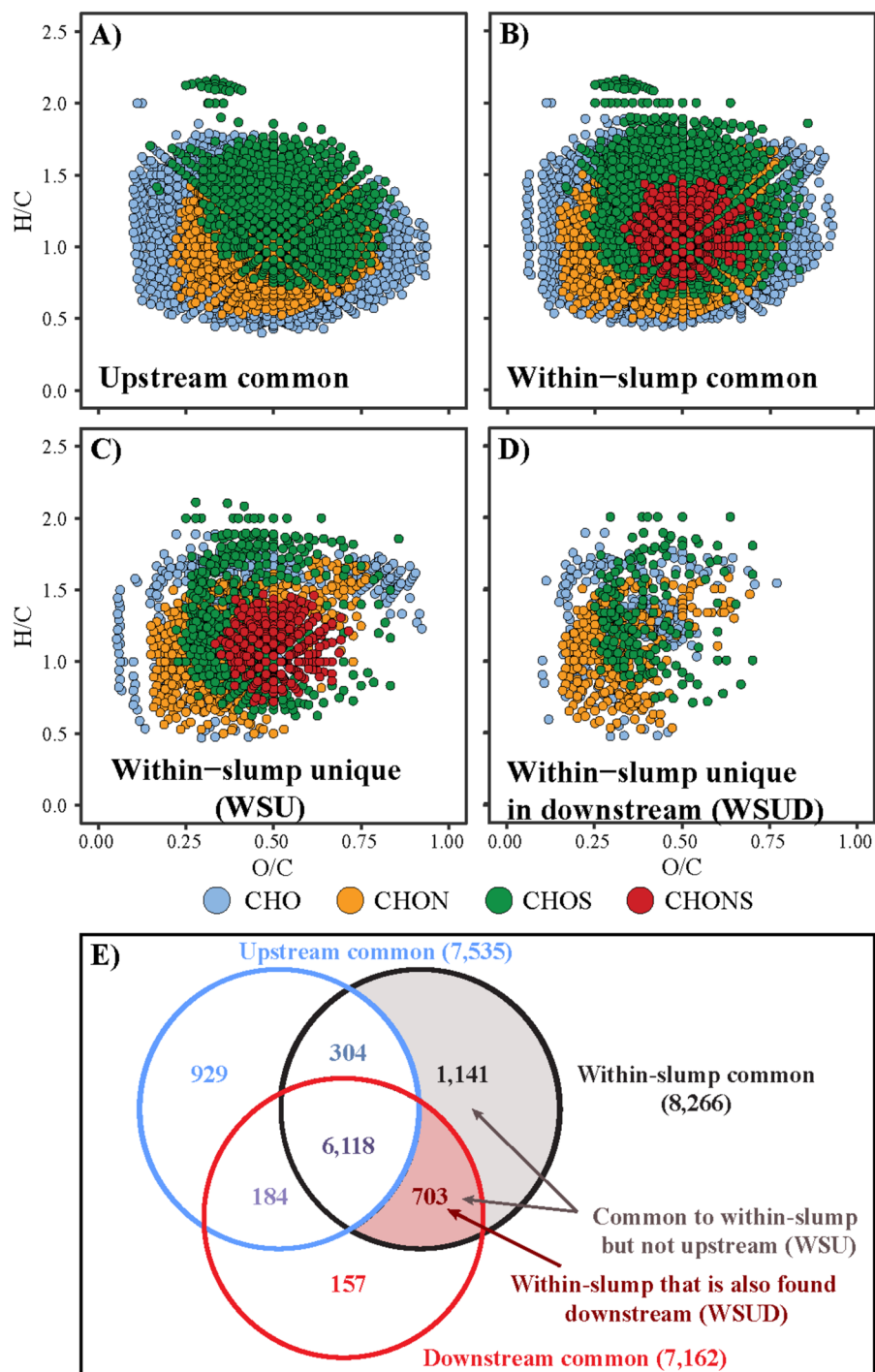
Tracing dissolved organic matter permafrost slump signals downstream

A PCA of FT-ICR MS and optically derived parameters resulted in two significant principal components, with PC1 explaining 58.4% of variance, and PC2 explaining 17.9% of variance within the dataset (Table 3 and Fig. 6). The main drivers that were positively associated with PC1 were AI$_{mod}$, HUP high O/C, NOSC, and CHO, and negatively aliphatics,

Table 4 Unique and common formulae for upstream, within-slump, and downstream locations

	Number	Mass	H/C	O/C	N/C *	S/C *	AImod	NOSC
Upstream common	7535	503.4139	1.11	0.48	19.55	7.08	0.32	− 0.08
Within-slump common	8266	484.7614	1.16	0.45	21.69	10.72	0.29	− 0.17
Within-slump unique (WSU)	1844	492.9517	1.23	0.42	30.74	20.50	0.24	− 0.26
Within-slump unique in downstream (WSUD)	703	501.2307	1.22	0.36	24.41	13.43	0.28	− 0.40

*Denotes scale is 10^{-3}

CHONS, CHOS and $S_{275-295}$; while HUP low O/C was the main positive driver for PC2 and condensed aromatics and polyphenolics the main negative drivers. Based on the PCA with the overlain sample points (Fig. 6b), it is readily apparent that PC1 is most strongly associated with sample location, with upstream locations clearly congregating positively on PC1, and within-slump locations plotting mostly negatively on this axis. Generally, downstream locations fall between upstream and within-slump locations from the same slump site and date. In contrast, PC2 appears to highlight the seasonality of the samples as a secondary driver, most notably for the upstream locations where early season samples plot more negatively on PC2. In general, westerly slumps with deeper headwalls (e.g., SE) plotted more negatively on PC1, while the sites located further east, or with shallower headwalls plotted more positively.

The assigned molecular formulae across all sample locations were separated into formulae that were common to all upstream locations (upstream common), common to all within-slump locations (within-slump common), formulae found in all within-slump locations but not upstream locations (within-slump unique: WSU), and the within-slump unique formula that were also found in the downstream sites (within-slump unique in downstream: WSUD) (Fig. 7; Table 4; Supplemental Table 1). The WSUD formulae group represents the unique molecular fingerprint of permafrost RTS features that persists to the downstream sampling location after any instream in-situ processing including: microbial degradation, photo-degradation, and abiotic processes such as sorption (Fig. 7d) (Collins et al. 1995; Kawahigashi et al. 2006; Littlefair and Tank 2018; Ward et al. 2017). Most notably, the WSU group had substantially greater N/C and S/C ratios, while the upstream common group had the lowest N/C and S/C ratios (Table 4). Transitioning into the WSUD, the CHONS formulae disappear from van Krevelen space when compared to the

WSU group (Fig. 7c and d). This may coincide with the nitrogen-limited nature of microbial remineralization in the Peel Plateau, and thus within-slump nitrogen inputs into the Peel River could increase microbial respiration rates upon thaw (Littlefair and Tank 2018). Alternatively, these CHONS formulae may be preferentially sorbing during transport and they represent regions of van Krevelen space that readily adsorb (Subdiaga et al. 2020).

The WSU and the WSUD van Krevelen diagrams are more aliphatic relative to the upstream common group, exhibiting greater H/C average values of 1.23 and 1.22 respectively in comparison to 1.11 (Fig. 7; Table 4). The upstream common group has a greater relative proportion of high O/C aromatic formulae in comparison to the WSU and WSUD as evidenced by higher O/C values, higher AI_{mod}, and lower NOSC values (Fig. 7; Table 4; Supplemental Table 1). The WSU fingerprint is considered the permafrost thaw signature for the sampled sites as it encapsulates the molecular formulae that are solely found in RTS derived inputs. The difference between the WSU and the WSUD groups may be caused by sorption to minerals as previously hypothesized in the region (Littlefair and Tank 2018), or utilization by microorganisms (Spencer et al. 2015; Vonk et al. 2013) or a combination of these processes. The potential for photochemical degradation at these study sites to be a driver of changes in DOM composition between WSU and WSUD would appear to be limited due to high suspended sediment loads (Shakil et al. 2020) and no selective loss of aromatic moieties as evidenced by no overall change in AI_{mod} (Table 4).

The patterns of molecular level composition observed between locations in this study complement past research on the Peel Plateau that found greater biolability in within-slump locations (Littlefair and Tank 2018), as past studies have found greater biolability in relatively more aliphatic samples (Spencer et al. 2015; Textor et al. 2019). Future projections

postulate a reduction in the extent of permafrost cover and a concurrent expansion of the active layer in soils in the Arctic with warming conditions (Lewkowicz and Way 2019; Schuur et al. 2008). As these conditions present themselves, an increase in thermokarst features including RTS can be expected to develop, and more within-slump conditions will be expected in the Peel Plateau (Lewkowicz and Way 2019; Kokelj et al. 2021). As thaw-slump derived DOM has been shown to have a greater prevalence of biolabile aliphatic formulae in this study, an increased relative contribution of aliphatic formulae to aquatic environments can be expected during conditions that favor the acceleration of thaw-driven mass wasting. Heterotrophic microbial degradation of aliphatic formulae has been shown to release greenhouse gases, however the balance between photosynthetic microbes and microbial respiration needs to be better quantified to assess the overall contribution to the global carbon cycle (Dutta and Dutta 2016). Furthermore, how these formulae will react when released into the downstream and coastal systems through riverine transport needs further study. Assessing the fate of this RTS DOM, it appears that some of this mobilized DOM may be sequestered through sorption to mineral surfaces and potentially buried in sedimentary deposits such as debris tongue or alluvial deposits (Littlefair et al. 2017). This compositionally distinct and energetically favorable DOM may also be rapidly utilized by microbial communities. However, to make these climatically relevant assessments both possibilities need to be examined further, and mechanistic sorption and bioincubation experiments undertaken incorporating ultrahigh resolution mass spectrometry to assess how DOM composition changes with these two mechanisms. Future studies linking WSUD formulae to biodegradable DOC would improve our understanding of how organic carbon from permafrost thaw is cycled through aquatic ecosystems and ultimately impacts the global carbon cycle. What is readily apparent from this study is that through utilizing FT-ICR MS it is possible to distinguish RTS DOM inputs into aquatic ecosystems in permafrost thaw-affected environments due to its unique molecular-level fingerprint, and that a portion of that unique fingerprint persists downstream. Utilizing this tracer will aid future studies seeking not just to track RTS permafrost inputs, but also examine how these inputs might be changing in a warming Arctic.

Declarations

Conflicts of interest The authors have no relevant conflicts of interest to disclose, financial or otherwise.

References

Abbott BW, Larouche JR, Jones JB, Bowden WB, Balser AW (2014) Elevated dissolved organic carbon biodegradability from thawing and collapsing permafrost. J Geophys Res Biogeosci 119(10):2049–2063. https://doi.org/10.1002/2014JG002678

Behnke MI, McClelland JW, Tank SE, Kellerman AM, Holmes RM, Haghipour N, Eglinton TI, Raymond PA, Suslova A, Zhulidov Av, Gurtovaya T, Zimov N, Zimov S, Mutter EA, Amos E, Spencer RGM (2021) Pan-Arctic Riverine Dissolved Organic Matter: Synchronous Molecular Stability Shifting Sources and Subsidies. Glob Biogeochem Cycles. https://doi.org/10.1029/2020GB006871

Biskaborn BK, Smith SL, Noetzli J, Matthes H, Vieira G, Streletskiy DA, Schoeneich P, Romanovsky VE, Lewkowicz AG, Abramov A, Allard M, Boike J, Cable WL, Christiansen HH, Delaloye R, Diekmann B, Drozdov D,

Etzelmüller B, Grosse G, Lantuit H (2019) Permafrost is warming at a global scale. Nat Commun 10(1):264. https://doi.org/10.1038/s41467-018-08240-4

Bröder L, Keskitalo K, Zolkos S, Shakil S, Tank SE, Kokelj Sv, Tesi T, van Dongen BE, Haghipour N, Eglinton TI, Vonk JE (2021) Preferential export of permafrost-derived organic matter as retrogressive thaw slumping intensifies. Environ Res Lett. https://doi.org/10.1088/1748-9326/abee4b

Burn CR (1997) Cryostratigraphy, paleogeography, and climate change during the early Holocene warm interval, western Arctic coast. Can Can J Earth Sci 34(7):912–925. https://doi.org/10.1139/e17-076

Collins MJ, Bishop AN, Farrimond P (1995) Sorption by mineral surfaces: Rebirth of the classical condensation pathway for kerogen formation? Geochim Cosmochim Acta 59(11):2387–2391. https://doi.org/10.1016/0016-7037(95)00114-F

Corilo, Y. (2015). PetroOrg. Florida State University.

de Haan H, de Boer T (1987) Applicability of light absorbance and fluorescence as measures of concentration and molecular size of dissolved organic carbon in humic Lake Tjeukemeer. Water Res 21(6):731–734. https://doi.org/10.1016/0043-1354(87)90086-8

Dittmar T, Koch B, Hertkorn N, Kattner G (2008) A simple and efficient method for the solid-phase extraction of dissolved organic matter (SPE-DOM) from seawater. Limnol Oceanogr Methods. https://doi.org/10.4319/lom.2008.6.230

Drake TW, Guillemette F, Hemingway JD, Chanton JP, Podgorski DC, Zimov NS, Spencer RGM (2018) The Ephemeral Signature of Permafrost Carbon in an Arctic Fluvial Network. J Geophys Res Biogeosci 123(5):1475–1485. https://doi.org/10.1029/2017JG004311

Duk-Rodkin, A. (1992). Surficial Geology, Fort McPherson-Bell River, Yukon-Northwest Territories. https://doi.org/10.4095/184002

Dutta H, Dutta A (2016) The microbial aspect of climate change. Energy Ecol Environ 1(4):209–232. https://doi.org/10.1007/s40974-016-0034-7

Environment Canada (2015) Canadian Climate Normals 1981–2010 Station Data.

Green SA, Blough NV (1994) Optical absorption and fluorescence properties of chromophoric dissolved organic matter in natural waters. Limnol Oceanogr 39(8):1903–1916. https://doi.org/10.4319/lo.1994.39.8.1903

Gruber S (2012) Derivation and analysis of a high-resolution estimate of global permafrost zonation. Cryosphere 6(1):221–233. https://doi.org/10.5194/tc-6-221-2012

Helms JR, Stubbins A, Ritchie JD, Minor EC, Kieber DJ, Mopper K (2008) Absorption spectral slopes and slope ratios as indicators of molecular weight, source, and photobleaching of chromophoric dissolved organic matter. Limnol Oceanogr 53(3):955–969. https://doi.org/10.4319/lo.2008.53.3.0955

Hendrickson CL, Quinn JP, Kaiser NK, Smith DF, Blakney GT, Chen T, Marshall AG, Weisbrod CR, Beu SC (2015) 21 Tesla Fourier Transform Ion Cyclotron Resonance Mass Spectrometer: A National Resource for Ultrahigh Resolution Mass Analysis. J Am Soc Mass Spectrum 26(9):1626–1632. https://doi.org/10.1007/s13361-015-1182-2

Kassambara AM, Mundt F (2017) Factoextra: Extract and visualize the results of multivariate data analyses. R package version 1(4)

Kawahigashi M, Kaiser K, Rodionov A, Guggenberger G (2006) Sorption of dissolved organic matter by mineral soils of the Siberian forest tundra. Glob Change Biol 12(10):1868–1877. https://doi.org/10.1111/j.1365-2486.2006.01203.x

Kellerman AM, Guillemette F, Podgorski DC, Aiken GR, Butler KD, Spencer RGM (2018) Unifying Concepts Linking Dissolved Organic Matter Composition to Persistence in Aquatic Ecosystems. Environ Sci Technol 52(5):2538–2548. https://doi.org/10.1021/acs.est.7b05513

Kokelj SV, Tunnicliffe J, Lacelle D, Lantz TC, Chin KS, Fraser R (2015) Increased precipitation drives mega slump development and destabilization of ice-rich permafrost terrain, northwestern Canada. Global Planet Change 129:56–68. https://doi.org/10.1016/j.gloplacha.2015.02.008

Kokelj SV, Kokoszka J, van der Sluijs J, Rudy ACA, Tunnicliffe J, Shakil S, Tank SE, Zolkos S (2021) Thaw-driven mass wasting couples slopes with downstream systems, and effects propagate through Arctic drainage networks. Cryosphere 15(7):3059–3081. https://doi.org/10.5194/tc-15-3059-2021

Kokelj Sv, Tunnicliffe JF, Lacelle D (2017) The Peel Plateau of Northwestern Canada: An Ice-Rich Hummocky Moraine Landscape in Transition, pp. 109–122. https://doi.org/10.1007/978-3-319-44595-3_7

Kurek MR, Stubbins A, Drake TW, Moura JMS, Holmes RM, Osterholz H, Dittmar T, Peucker-Ehrenbrink B, Mitsuya M, Spencer RGM (2021) Drivers of Organic Molecular Signatures in the Amazon River. Glob Biogeochem Cycles. https://doi.org/10.1029/2021GB006938

Kurek MR, Frey KE, Guillemette F, Podgorski DC, Townsend-Small A, Arp CD, Kellerman AM, Spencer RGM (2022a) Trapped Under Ice: Spatial and Seasonal Dynamics of Dissolved Organic Matter Composition in Tundra Lakes. J Geophys Res Biogeosci. https://doi.org/10.1029/2021JG006578

Kurek MR, Stubbins A, Drake TW, Dittmar TMS, Moura J, Holmes RM, Osterholz H, Six J, Wabakanghanzi JN, Dinga B, Mitsuya M, Spencer RGM (2022b) Organic molecular signatures of the Congo river and comparison to the Amazon. Glob Biogeochem Cycles. https://doi.org/10.1029/2022GB007301

Kurek MR, Garcia-Tigreros F, Wickland KP, Frey KE, Dornblaser MM, Striegl RG, Niles SF, McKenna AM, Aukes PJK, Kyzivat ED, Wang C, Pavelsky TM, Smith LC, Schiff SL, Butman D, Spencer RGM (2023) Hydrologic and Landscape Controls on Dissolved Organic Matter Composition Across Western North American Arctic Lakes. Glob Biogeochem Cycles. https://doi.org/10.1029/2022GB007495

Lacelle D, Lauriol B, Zazula G, Ghaleb B, Utting N, Clark ID (2013) Timing of advance and basal condition of the Laurentide Ice Sheet during the last glacial maximum in the Richardson Mountains. NWT Q Res 80(2):274–283. https://doi.org/10.1016/j.yqres.2013.06.001

LaRowe DE, van Cappellen P (2011) Degradation of natural organic matter: A thermodynamic analysis. Geochim Cosmochim Acta 75(8):2030–2042. https://doi.org/10.1016/j.gca.2011.01.020

Leewis M-C, Berlemont R, Podgorski DC, Srinivas A, Zito P, Spencer RGM, McFarland J, Douglas TA, Conaway CH, Waldrop M, Mackelprang R (2020) Life at the Frozen Limit: Microbial Carbon Metabolism Across a Late Pleistocene Permafrost Chronosequence. Front Microbiol. https://doi.org/10.3389/fmicb.2020.01753

Lewkowicz AG, Way RG (2019) Extremes of summer climate trigger thousands of thermokarst landslides in a High Arctic environment. Nat Commun 10(1):1329. https://doi.org/10.1038/s41467-019-09314-7

Littlefair CA, Tank SE (2018) Biodegradability of Thermokarst Carbon in a Till-Associated, Glacial Margin Landscape: The Case of the Peel Plateau, NWT. Can J Geophys Res Biogeosci 123(10):3293–3307. https://doi.org/10.1029/2018JG004461

Littlefair CA, Tank SE, Kokelj Sv (2017) Retrogressive thaw slumps temper dissolved organic carbon delivery to streams of the Peel Plateau, NWT. Can Biogeosci 14(23):5487–5505. https://doi.org/10.5194/bg-14-5487-2017

Mann PJ, Davydova A, Zimov N, Spencer RGM, Davydov S, Bulygina E, Zimov S, Holmes RM (2012) Controls on the composition and lability of dissolved organic matter in Siberia's Kolyma River basin. J Geophys Res Biogeosci. https://doi.org/10.1029/2011JG001798

Mooshammer M, Wanek W, Hämmerle I, Fuchslueger L, Hofhansl F, Knoltsch A, Schnecker J, Takriti M, Watzka M, Wild B, Keiblinger KM, Zechmeister-Boltenstern S, Richter A (2014) Adjustment of microbial nitrogen use efficiency to carbon:nitrogen imbalances regulates soil nitrogen cycling. Nat Commun 5(1):3694. https://doi.org/10.1038/ncomms4694

Murphy KR, Stedmon CA, Graeber D, Bro R (2013) Fluorescence spectroscopy and multi-way techniques. PARAFAC. Anal Methods. https://doi.org/10.1039/c3ay41160e

Obu J (2021) How Much of the Earth's Surface is Underlain by Permafrost? J Geophys Res Earth Surface. https://doi.org/10.1029/2021JF006123

Olefeldt D, Roulet NT (2012) Effects of permafrost and hydrology on the composition and transport of dissolved organic carbon in a subarctic peatland complex. J Geophys Res Biogeosci. https://doi.org/10.1029/2011JG001819

O'Neill HB, Burn CR, Kokelj SV, Lantz TC (2015) 'Warm' Tundra: Atmospheric and Near-Surface Ground Temperature Inversions Across an Alpine Treeline in Continuous Permafrost, Western Arctic. Can Permafrost Periglacial Processes 26(2):103–118. https://doi.org/10.1002/ppp.1838

Peter S, Shen Y, Kaiser K, Benner R, Durisch-Kaiser E (2012) Bioavailability and diagenetic state of dissolved organic matter in riparian groundwater. J Geophys Res Biogeosci. https://doi.org/10.1029/2012JG002072

Peuravuori J, Pihlaja K (1997) Molecular size distribution and spectroscopic properties of aquatic humic substances. Anal Chim Acta 337(2):133–149. https://doi.org/10.1016/S0003-2670(96)00412-6

R Core Team (2019) A language and environment for statistical computing. R Foundation for Statistical Computing (https://www.R-project.org/)

Richter-Menge J, Druckenmiller ML, Jeffries M (2019) Arctic Report Card 2019

Rogers JA, Galy V, Kellerman AM, Chanton JP, Zimov N, Spencer RGM (2021) Limited Presence of Permafrost Dissolved Organic Matter in the Kolyma River, Siberia Revealed by Ramped Oxidation. J Geophys Res Biogeosci. https://doi.org/10.1029/2020JG005977

Šantl-Temkiv T, Finster K, Dittmar T, Hansen BM, Thyrhaug R, Nielsen NW, Karlson UG (2013) Hailstones: A Window into the Microbial and Chemical Inventory of a Storm Cloud. PLoS ONE 8(1):e53550. https://doi.org/10.1371/journal.pone.0053550

Schmidt F, Elvert M, Koch BP, Witt M, Hinrichs K-U (2009) Molecular characterization of dissolved organic matter in pore water of continental shelf sediments. Geochim Cosmochim Acta 73(11):3337–3358. https://doi.org/10.1016/j.gca.2009.03.008

Schuur E, Bockham J, Canadell J (2008) Vulnerability of Permafrost Carbon to Climate Change: Implications for the Global Carbon Cycle. Bioscience 58:701

Shakil S, Tank SE, Kokelj SV, Vonk JE, Zolkos S (2020) Particulate dominance of organic carbon mobilization from thaw slumps on the Peel Plateau, NT: Quantification and implications for stream systems and permafrost carbon release. Environ Res Lett 15(11):114019. https://doi.org/10.1088/1748-9326/abac36

Sinsabaugh RL, Turner BL, Talbot JM, Waring BG, Powers JS, Kuske CR, Moorhead DL, Follstad Shah JJ (2016) Stoichiometry of microbial carbon use efficiency in soils. Ecol Monogr 86(2):172–189. https://doi.org/10.1890/15-2110.1

Sistla SA, Asao S, Schimel JP (2012) Detecting microbial N-limitation in tussock tundra soil: Implications for Arctic soil organic carbon cycling. Soil Biol Biochem 55:78–84. https://doi.org/10.1016/j.soilbio.2012.06.010

Sleighter RL, Hatcher PG (2008) Molecular characterization of dissolved organic matter (DOM) along a river to ocean transect of the lower Chesapeake Bay by ultrahigh resolution electrospray ionization Fourier transform ion cyclotron resonance mass spectrometry. Mar Chem 110(3–4):140–152. https://doi.org/10.1016/j.marchem.2008.04.008

Smith DF, Podgorski DC, Rodgers RP, Blakney GT, Hendrickson CL (2018) 21 Tesla FT-ICR Mass Spectrometer for Ultrahigh-Resolution Analysis of Complex Organic Mixtures. Anal Chem 90(3):2041–2047. https://doi.org/10.1021/acs.analchem.7b04159

Spencer RGM, Baker A, Ahad JME, Cowie GL, Ganeshram R, Upstill-Goddard RC, Uher G (2007) Discriminatory classification of natural and anthropogenic waters in two U.K. estuaries. Sci Total Environ 373(1):305–323. https://doi.org/10.1016/j.scitotenv.2006.10.052

Spencer RGM, Butler KD, Aiken GR (2012) Dissolved organic carbon and chromophoric dissolved organic matter properties of rivers in the USA. J Geophys Res Biogeosci. https://doi.org/10.1029/2011JG001928

Spencer RGM, Mann PJ, Dittmar T, Eglinton TI, McIntyre C, Holmes RM, Zimov N, Stubbins A (2015) Detecting the signature of permafrost thaw in Arctic rivers. Geophys Res Lett 42(8):2830–2835. https://doi.org/10.1002/2015GL063498

Subdiaga E, Harir M, Orsetti S, Hertkorn N, Schmitt-Kopplin P, Haderlein SB (2020) Preferential Sorption of Tannins at Aluminum Oxide Affects the Electron Exchange Capacities of Dissolved and Sorbed Humic Acid Fractions. Environ Sci Technol 54(3):1837–1847. https://doi.org/10.1021/acs.est.9b04733

Textor SR, Wickland KP, Podgorski DC, Johnston SE, Spencer RGM (2019) Dissolved Organic Carbon Turnover in Permafrost-Influenced Watersheds of Interior Alaska: Molecular Insights and the Priming Effect. Front Earth Sci. https://doi.org/10.3389/feart.2019.00275

The Physical Science Basis Summary for Policymakers Working Group I contribution to the Sixth Assessment Report of the Intergovernmental Panel on Climate Change. (2021).

van der Sluijs J (2023) Allometric scaling of retrogressive thaw slumps. Eu Geosci Union: Cryosphere 17(11):4511–4533. https://doi.org/10.5194/tc-17-4511-2023

Vaughn DR, Kellerman AM, Wickland KP, Striegl RG, Podgorski DC, Hawkings JR, Nienhuis JH, Dornblaser MM, Stets EG, Spencer RGM (2021) Anthropogenic landcover impacts fluvial dissolved organic matter composition in the Upper Mississippi River Basin. Biogeochemistry. https://doi.org/10.1007/s10533-021-00852-1

Vonk JE, Mann PJ, Davydov S, Davydova A, Spencer RGM, Schade J, Sobczak WV, Zimov N, Zimov S, Bulygina E, Eglinton TI, Holmes RM (2013) High biolability of ancient permafrost carbon upon thaw. Geophys Res Lett 40(11):2689–2693. https://doi.org/10.1002/grl.50348

Vonk JE, Tank SE, Bowden WB, Laurion I, Vincent WF, Alekseychik P, Amyot M, Billet MF, Canário J, Cory RM, Deshpande BN, Helbig M, Jammet M, Karlsson J, Larouche J, Macmillan G, Rautio M, Walter Anthony KM, Wickland KP (2015) Reviews and syntheses: Effects of permafrost thaw on Arctic aquatic ecosystems. In Biogeosciences (Vol. 12, Issue 23, pp. 7129–7167). Copernicus GmbH. 10.5194/bg-12-7129-2015

Vonk JE, Tank SE, Mann PJ, Spencer RGM, Treat CC, Striegl RG, Abbott BW, Wickland KP (2015b) Biodegradability of dissolved organic carbon in permafrost soils and aquatic systems: A meta-analysis. Biogeosciences 12(23):6915–6930. https://doi.org/10.5194/bg-12-6915-2015

Wagner S, Riedel T, Niggemann J, Vähätalo AV, Dittmar T, Jaffé R (2015) Linking the Molecular Signature of Heteroatomic Dissolved Organic Matter to Watershed Characteristics in World Rivers. Environ Sci Technol 49(23):13798–13806. https://doi.org/10.1021/acs.est.5b00525

Ward CP, Nalven SG, Crump BC, Kling GW, Cory RM (2017) Photochemical alteration of organic carbon draining permafrost soils shifts microbial metabolic pathways and stimulates respiration. Nat Commun. https://doi.org/10.1038/s41467-017-00759-2

Weishaar JL, Aiken GR, Bergamaschi BA, Fram MS, Fujii R, Mopper K (2003) Evaluation of Specific Ultraviolet Absorbance as an Indicator of the Chemical Composition and Reactivity of Dissolved Organic Carbon. Environ Sci Technol 37(20):4702–4708. https://doi.org/10.1021/es030360x

Wickham H (2016) ggplot2: elegant graphics for data analysis. springer.

Wild B, Schnecker J, Knoltsch A, Takriti M, Mooshammer M, Gentsch N, Mikutta R, Alves RJE, Gittel A, Lashchinskiy N, Richter A (2015) Microbial nitrogen dynamics in organic and mineral soil horizons along a latitudinal transect in western Siberia. Glob Biogeochem Cycles 29(5):567–582. https://doi.org/10.1002/2015GB005084

Zolkos S, Tank SE (2019) Permafrost Geochemistry and Retrogressive Thaw Slump Morphology (Peel Plateau, Canada)

Zolkos S, Tank SE, Kokelj SV (2018) Mineral Weathering and the Permafrost Carbon-Climate Feedback. Geophys Res Lett 45(18):9623–9632. https://doi.org/10.1029/2018GL078748

Zolkos S, Tank SE, Striegl RG, Kokelj S, v. (2019) Thermokarst Effects on Carbon Dioxide and Methane Fluxes in Streams on the Peel Plateau (NWT, Canada). J Geophys Res Biogeosci 124(7):1781–1798. https://doi.org/10.1029/2019JG005038